Mutation-independent rhodopsin gene therapy by knockdown and replacement with a single AAV vector

Artur V. Cideciyan[a,1], Raghavi Sudharsan[b], Valérie L. Dufour[b], Michael T. Massengill[c], Simone Iwabe[b], Malgorzata Swider[a], Brianna Lisi[a], Alexander Sumaroka[a], Luis Felipe Marinho[b], Tatyana Appelbaum[b], Brian Rossmiller[c], William W. Hauswirth[d], Samuel G. Jacobson[a], Alfred S. Lewin[c,2], Gustavo D. Aguirre[b], and William A. Beltran[b,1,2]

[a]Scheie Eye Institute, Department of Ophthalmology, University of Pennsylvania Perelman School of Medicine, Philadelphia, PA 19104; [b]Division of Experimental Retinal Therapies, Department of Clinical Sciences and Advanced Medicine, School of Veterinary Medicine, University of Pennsylvania, Philadelphia, PA 19104; [c]Department of Molecular Genetics and Microbiology, University of Florida, Gainesville, FL 32610; and [d]Department of Ophthalmology, University of Florida, Gainesville, FL 32610

Inherited retinal degenerations are caused by mutations in >250 genes that affect photoreceptor cells or the retinal pigment epithelium and result in vision loss. For autosomal recessive and X-linked retinal degenerations, significant progress has been achieved in the field of gene therapy as evidenced by the growing number of clinical trials and the recent commercialization of the first gene therapy for a form of congenital blindness. However, despite significant efforts to develop a treatment for the most common form of autosomal dominant retinitis pigmentosa (adRP) caused by >150 mutations in the rhodopsin (RHO) gene, translation to the clinic has stalled. Here, we identified a highly efficient shRNA that targets human (and canine) RHO in a mutation-independent manner. In a single adeno-associated viral (AAV) vector we combined this shRNA with a human RHO replacement cDNA made resistant to RNA interference and tested this construct in a naturally occurring canine model of RHO-adRP. Subretinal vector injections led to nearly complete suppression of endogenous canine RHO RNA, while the human RHO replacement cDNA resulted in up to 30% of normal RHO protein levels. Noninvasive retinal imaging showed photoreceptors in treated areas were completely protected from retinal degeneration. Histopathology confirmed retention of normal photoreceptor structure and RHO expression in rod outer segments. Long-term (>8 mo) follow-up by retinal imaging and electroretinography indicated stable structural and functional preservation. The efficacy of this gene therapy in a clinically relevant large-animal model paves the way for treating patients with RHO-adRP.

autosomal dominant retinitis pigmentosa | retinal degeneration | gene therapy | RHO | RNA interference

The past two decades have seen a steep rise in the number of gene therapies entering clinical trials (1, 2), and in recent years a small number of them have received marketing approval by regulatory authorities in China, Europe, and the United States (3). The great majority of these trials have targeted cancer, cardiovascular, and inherited monogenic diseases (1). Strategies for inherited monogenic diseases are by necessity based on the mechanism of disease. For the great majority of loss-of-function mutations, the strategy is gene augmentation (4). For mutations that cause a dominant-negative effect, gene augmentation may also provide some therapeutic benefit by diluting the deleterious effect of the mutant product (5, 6). However, in the case of mutations that confer a toxic gain of function, strategies that are being investigated include ablation of the gene or correction of the defect at the DNA level (e.g., CRISPR/Cas9 gene editing), transcriptional repression, and RNA knockdown/suppression (7, 8).

Mutations in more than 250 genes are known to cause inherited retinal diseases (https://sph.uth.edu/retnet/), and considerable advances have been made in gene therapy approaches because of the accessibility of the retina. Clinical trials of gene augmentation are currently ongoing for at least six autosomal recessive diseases, three X-linked diseases, and one maternally inherited mitochondrial retinal disease (9). There are no trials for autosomal dominant retinal diseases, the most common of which is autosomal dominant retinitis pigmentosa (adRP) caused by mutations in the rhodopsin (RHO) gene (10–14). For the more than 150 identified RHO mutations, several putative pathogenic mechanisms based mostly on in vitro findings have been proposed (for review see refs. 15 and 16), but detailed characterization of RHO-adRP patient phenotype is consistent with two major categories (17–19). Patients with class A mutations have severe loss of rods from early life, and realistic therapeutic approaches should be directed at prolonging cone survival. On the other hand, patients with class B mutations can have rods that survive for decades into late adult life in some retinal regions or throughout the retina and could benefit from a gene therapy aimed at rescuing the remaining rods and preventing secondary cone cell loss (20).

Over the past 20 years, efforts in gene therapy for RHO-adRP have focused on either reducing the expression of specific mutant alleles (21–28) or developing a mutation-independent strategy. The latter strategy combines knocking down the expression of

Significance

A number of gene-augmentation strategies are entering clinical trials for the treatment of inherited retinal blindness. Gene therapy for autosomal dominant diseases faces significant obstacles that include allelic heterogeneity and the potential need to silence the mutated gene. Here we show that a single-gene therapy vector that combines knockdown of the causative gene with its replacement by a resistant wild-type copy can prevent photoreceptor cell death and vision loss in a canine model of autosomal dominant retinitis pigmentosa.

both the mutant and WT RHO proteins (29–39) while providing a resistant *RHO* cDNA that encodes for the WT protein (40–43) as a replacement. Resistance is conferred by codon modification at degenerate/wobble nucleotides within the target site, which prevents hybridization with the knockdown reagent. Such a mutation-independent knockdown-and-replacement strategy aims at addressing the high allelic heterogeneity in *RHO*-adRP while circumventing the technical and financial challenges that would be inherent in developing multiple gene therapies for individual *RHO* mutations. The retinal codelivery of the two components using either two separate (42), or a single adeno-associated viral (AAV) vector (41, 43) have been explored in transgenic mice by separate research groups. However, complete prevention or arrest of the ongoing rod degeneration was not achieved.

In the present study we identified a highly effective shRNA that targets human *RHO* in a mutation-independent manner. When combined with a resistant form of human *RHO* and copackaged in a single recombinant AAV vector, this vector with dual knockdown and replacement functions provided long-term protection against retinal degeneration in a naturally occurring canine model of *RHO*-adRP.

Results

Optimal Suppression of WT Rhodopsin with shRNA$_{820}$. Four knockdown reagents, a previously identified (33) hammerhead ribozyme (*Rz525*) and three shRNAs (*shRNA$_{131}$*, *shRNA$_{134}$*, and *shRNA$_{820}$*) that target distinct homologous regions of canine and human RHO (*SI Appendix*, Fig. S1), were screened initially using in vitro assays. Silencing of RHO expression was very effective with *Rz525* both in vitro (*SI Appendix*, Fig. S2) and in WT (*SI Appendix*, Fig. S3 and Table S1 group C) and *RHO*-mutant canine eyes (*SI Appendix*, Fig. S4 *A–C* and Table S1 group F). However, due to severe retinal complications associated with the high viral titers of AAV2/5-*Rz525* needed to achieve nearly

complete suppression of RHO expression (*SI Appendix, Supplemental Results* and Fig. S4 *D* and *E*), further development of Rz525 was discontinued. In vitro screening of shRNAs showed that *shRNA$_{131}$* resulted in only an ~50% reduction of WT human RHO protein (Fig. 1 *A* and *B*) and failed to suppress mutant human RHO P23H (Fig. 1 *C* and *D*) and T17M (Fig. 1 *E* and *F*). Moreover, there was limited suppression of RHO expression in injected canine WT eyes (*SI Appendix, Supplemental Results*, Fig. S5, and Table S1 group B).

The shRNA that most potently suppressed expression of both WT and mutant (P23H and T17M) human RHO protein in vitro was *shRNA$_{820}$* (Fig. 1 *A–F*). In parallel, a codon-modified form of human *RHO*, *RHO$_{820}$*, that contained four altered nucleotides at degenerate/wobble positions within the target site of *shRNA$_{820}$* was confirmed to be resistant to *shRNA$_{820}$* suppression (Fig. 1 *G* and *H*). Once it was confirmed that *shRNA$_{820}$* targeted *RHO* in a mutation-independent manner, *shRNA$_{820}$* was selected as the lead knockdown reagent and was packaged in an AAV2/5 vector under the control of the H1 RNA promoter for further evaluation in WT and *RHO*-mutant dogs.

Validation of *shRNA$_{820}$* was performed first in WT dogs to determine the titer at which RHO expression can be substantially reduced with expected changes occurring only in outer segments, where RHO is a major signaling and structural protein, but without major stress or degeneration of the remaining cellular compartments of rod photoreceptors. Subretinal injections with AAV-*shRNA820* titers ranging from 1×10^{11} to 50×10^{11} viral genomes (vg)/mL were performed in 10 WT canine eyes (*SI Appendix*, Table S1 group A). Treated eyes were evaluated at 7–8 wk postinjection by in vivo optical coherence tomography (OCT) imaging of the retinal structure and were compared with uninjected control eyes. In a representative uninjected WT eye, cross-sectional imaging in the superior retina with OCT revealed hypo- and hyper-scattering layers corresponding to different
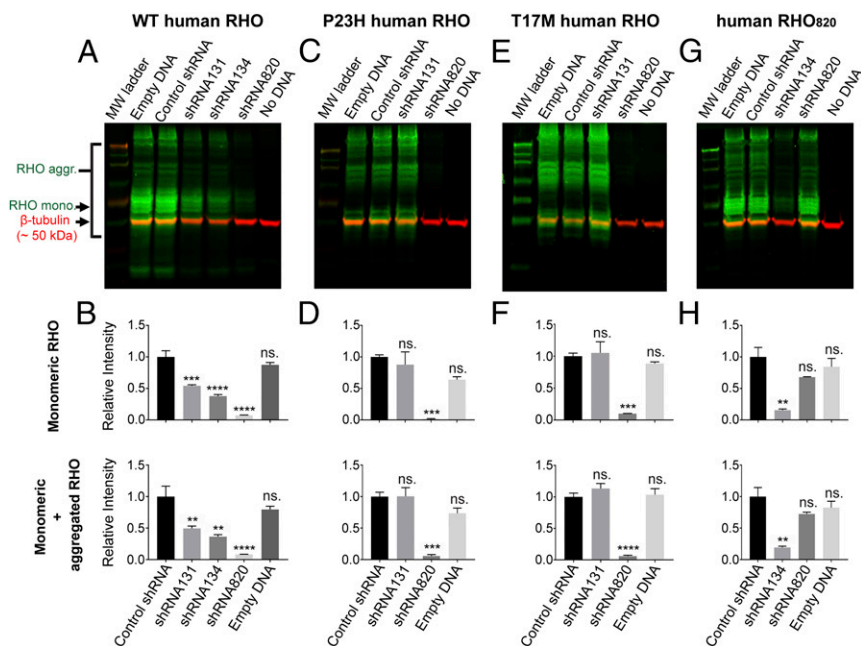
Fig. 1. shRNA-mediated knockdown of WT, P23H, T17M, and *shRNA820*-resistant (*RHO$_{820}$*) variants of human *RHO*. HEK293T cells were transfected with a plasmid expressing WT, P23H, T17M, or *shRNA820*-resistant (*RHO$_{820}$*) human *RHO* with a C-terminal turboGFP tag (*RHO-tGFP*) and with a rAAV2 plasmid (denoted in lane labels) encoding empty DNA (no shRNA), a control *shRNA*, *shRNA$_{131}$*, *shRNA$_{134}$*, or *shRNA$_{820}$*. A no-DNA transfection control was also included. (*A*, *C*, *E*, and *G*) Immunoblots of protein samples isolated from transfected HEK293T cells probed for turboGFP tag (green) and β-tubulin (red) as the loading control. Rho aggr., aggregated form of RHO-GFP; Rho mono., monomeric form of RHO-GFP. (*B*, *D*, *F*, and *H*) Relative quantification of the monomeric form of RHO-GFP (*Upper*) and of the monomeric and aggregated forms of RHO-GFP (*Lower*). The first lane of each Western blot contained the Chameleon Duo Prestained Protein Ladder from Li-Cor. Bars denote the mean value of three technical replicates; error bars denote SEM. ns, not significant, **$P < 0.01$, ***$P < 0.001$, ****$P < 0.0001$.

scAAV2/5-H1-shRNA$_{820}$ in WT
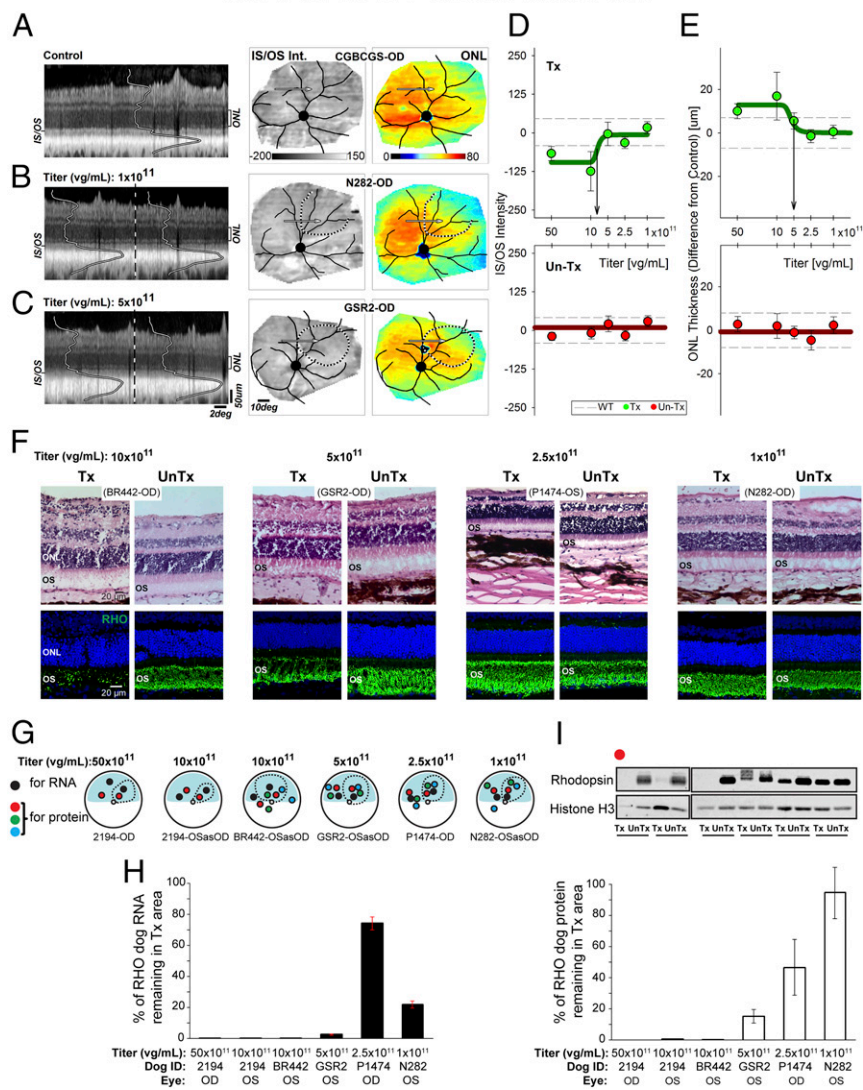
Fig. 2. Suppression of rhodopsin with *shRNA*$_{820}$ in WT retinas. (*A–C*) In vivo imaging results from representative WT eyes 7–8 wk postinjection with scAAV2/5-H1-*shRNA*$_{820}$ at 1×10^{11} (*B*) and 5×10^{11} vg/mL (*C*) titers compared with uninjected control (*A*). Shown are OCT scans (*Left*), normalized IS/OS intensity topography (*Center*), and ONL thickness topography (*Right*). Dotted lines indicate injection bleb boundaries. Arrows indicate the location of the OCTs shown on left. (*D* and *E*) Normalized IS/OS intensity (*D*) and ONL thickness (*E*) sampled within the injected blebs (green symbols, *Upper*) and uninjected control locations (red symbols, *Lower*) in 10 eyes injected with a range of titers. Symbols represent group averages ($\pm$ SD) from 33–95 samples (*SI Appendix*, Fig. S6). Dashed lines denote the 99th percentile limits of the respective parameters sampled at the same retinal locations in uninjected control eyes. Downward arrows estimate the titers corresponding to the transitions to a detectable effect. (*F*) Microphotographs of H&E-stained (*Upper*) and rhodopsin (RHO, green) immunolabeled (*Lower*) retinal cryosections showing the morphology of the ONL and outer segments (OS) in areas treated with 1×10^{11} to 10×10^{11} vg/mL titer range (Tx) and untreated areas (UnTx) 7–8 wk postinjection. (*G*) Schematic representation of the retinas of WT dogs treated with 1×10^{11} to 50×10^{11} vg/mL titers showing the location of neuroretinal punches used for quantification of rhodopsin (RNA and protein) expression 7–8 wk postinjection. Dashed lines indicate bleb boundaries; the blue area indicates the tapetal region. (*H*) Quantification of the levels of endogenous canine *RHO* RNA remaining in the treated retinal area as a percentage of levels measured in the untreated area of eyes injected with the different vector titers. (*I*) Representative immunoblot and quantification of the levels of endogenous canine RHO protein remaining in the treated retinal area as a percentage of levels measured in the untreated area of eyes injected with the different vector titers. Labels such as N282-OD refer to the animal and the eye; OSasOD indicates the left eye is displayed as the right eye for comparability.

NEUROSCIENCE

retinal lamina (Fig. 2*A*, *Left*) (44). The thickness of the outer nuclear layer (ONL) where the photoreceptor nuclei reside and the backscatter intensity originating near the inner segment–outer segment (IS/OS) junction were of primary interest in this study (Fig. 2*A*, *Left*). IS/OS intensity is expected to be sensitive to changes in outer segment length, alignment, and spatial density and thus can be used as a noninvasive surrogate measure of outer segment health. The normalized IS/OS intensity topography of the uninjected WT eye tends to be uniform (Fig. 2*A*, *Center*). ONL thickness topography in the uninjected WT eye was also relatively homogeneous with incrementally greater values in the central retina supero-temporal to the optic nerve head (ONH) and incrementally smaller values in the nontapetal areas of superior and inferior retina (Fig. 2*A*, *Right*). Eyes with lower (1×10^{11} vg/mL) (Fig. 2*B*) and intermediate (5×10^{11} vg/mL) (Fig. 2*C*) titer injections showed no qualitative structural changes between the injected and neighboring uninjected regions.

To define the optimal titer at which structural consequences of RHO knockdown are detectable but mild, retinal locations were systematically sampled (*SI Appendix*, Fig. S6). The IS/OS intensity and ONL thickness in a great majority of the locations injected with the two lowest titers (1×10^{11} and 2.5×10^{11} vg/mL) were comparable to those in uninjected control eyes (Fig. 2 *D*

and *E*, *Upper*). In contrast, eyes injected with 10×10^{11} vg/mL showed the reduced IS/OS intensity expected from RHO knockdown (Fig. 2*D*) and some ONL thickening suggesting a subclinical response to the vector administration (Fig. 2*E*). Eyes injected with the highest titer (50×10^{11} vg/mL) showed vascular engorgement and infiltration of inflammatory cells in the vitreous; there also were abnormalities on cross-sectional imaging (Fig. 2 *D* and *E* and *SI Appendix*, Fig. S6). Transition to detectable changes occurred between 5×10^{11} and 8×10^{11} vg/mL (Fig. 2 *D* and *E*, arrows), suggesting a range of potential effective titers. The great majority of the loci at uninjected sites in the treated eyes at all titers were consistent with results expected from uninjected eyes, confirming that the effects of RHO knockdown were localized to the area of the subretinal injection (Fig. 2 *D* and *E*, *Lower*).

Animals were humanely killed at 7–8 wk postinjection, and four eyes that had been treated with titers ranging from 1×10^{11} to 10×10^{11} vg/mL were processed for histology and rhodopsin immunohistochemistry (Fig. 2*F*). Loss of outer segment structure associated with a prominent reduction in rod opsin immunolabeling was seen in the area treated with the 10×10^{11} vg/mL titer vector. There was also some detectable infiltration of inflammatory cells around retinal vessels, in the inner retina, and in the subretinal

space (Fig. 2F, Upper). At 5×10^{11} vg/mL some shortening of outer segments and reduction of rod opsin immunolabeling was found in the treated area compared with the untreated area of the same eye. At the two lowest titers (1×10^{11} and 2.5×10^{11} vg/mL), outer segments were preserved, and rod opsin immunolabeling was comparable between treated and untreated areas. The remaining six eyes injected with titers ranging from 1×10^{11} to 50×10^{11} vg/mL (Fig. 2G) were used to assess the efficiency of AAV-$shRNA_{820}$ in reducing the expression of endogenous canine RHO at both the RNA and protein levels. Absolute RNA quantification (Fig. 2H) showed very low levels of RHO transcripts (0–3% of that found in untreated areas) in the treated areas of eyes injected with titers ranging from 50×10^{11} down to 5×10^{11} vg/mL. At lower titers (1×10^{11} to 2.5×10^{11} vg/mL) knockdown efficiency was reduced, with 22–74% of normal RHO RNA levels still remaining in the treated areas. Quantification of RHO protein persisting in the treated areas on immunoblots revealed a dose-dependent effect (Fig. 2I), with undetectable levels in eyes treated with the two highest titers (50×10^{11} and 10×10^{11} vg/mL), 15% in the eye treated with 5×10^{11} vg/mL, and >47% in eyes treated with the two lowest titers.

These studies showed that subretinal AAV vector delivery of $shRNA_{820}$ can achieve very efficient silencing of WT canine RHO and suggested that the 5×10^{11} vg/mL titer may provide the optimal balance between the knockdown of a highly expressed structural protein in rod photoreceptors and retention of retinal integrity.

Suppression of Mutant RHO with $shRNA_{820}$. To verify the efficiency of $shRNA_{820}$ in heterozygous mutant retinas that express both WT and mutant RHO alleles, subretinal injections of AAV-$shRNA_{820}$ were performed over a range of titers (1×10^{11} to 10×10^{11} vg/mL) in 10 RHO-mutant eyes that were followed for 8–10 wk postinjection (SI Appendix, Table S1 groups D and E) Since the RHO-mutant dog retinas are highly sensitive to light (45–48), the animals were housed under dim red light from birth until the end of the study, and the surgical intervention was performed under infrared illumination (49). Four eyes were used for quantification of RHO knockdown efficiency at the RNA and protein levels (Fig. 3A and SI Appendix, Table S1 group D). As in the WT animals, at a titer of 10×10^{11} vg/mL there was complete silencing of RHO RNA and protein expression in the treated area (Fig. 3 B and C). A similar absence of RHO expression was achieved with the lower (5×10^{11} vg/mL) titer. However, interpretation of this result was confounded by OCT imaging revealing a partial loss of ONL thickness restricted to the treated area in this eye. Persistent expression of RHO was seen with the lower (1×10^{11} and 2.5×10^{11} vg/mL) titers.

Next, we evaluated whether knockdown alone could arrest photoreceptor degeneration. Another set of four RHO-mutant eyes (SI Appendix, Table S1 group E) were also injected with the same range of titers of AAV-$shRNA_{820}$, but at 6–8 wk postinjection they were exposed for 1 min to moderate-intensity white light known to cause acute retinal degeneration in this canine model (46–48). Two weeks after light exposure, the eye injected with the titers of 10×10^{11} and 5×10^{11} vg/mL showed a distinct region of ONL retention corresponding to the treatment area (Fig. 3D). Severe retinal degeneration outside the treatment area demonstrated the substantial rescue of photoreceptors achieved by knockdown alone. There were abnormalities with IS/OS intensity expected from the knockdown of RHO. Also, the eye injected with the highest (10×10^{11} vg/mL) titer showed some ONL thickening. Eyes injected with the two lowest titers
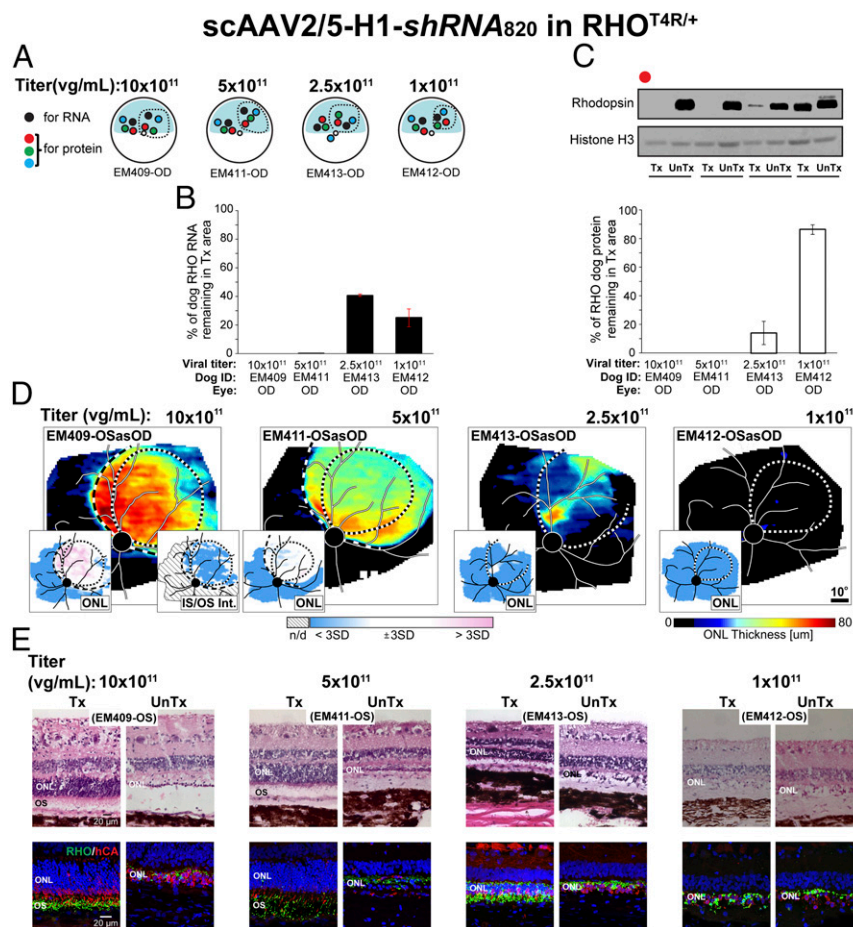

Fig. 3. Suppression of rhodopsin with $shRNA_{820}$ in RHO-mutant retinas. (A) Schematic representation of the fundus of four RHO-mutant dog eyes injected with scAAV2/5-H1-$shRNA_{820}$ at 1×10^{11} to 10×10^{11} vg/mL titers showing the location of neuroretinal punches used for quantification of rhodopsin (RNA and protein) expression at 8–10 wk postinjection. Dashed lines indicate bleb boundaries; the blue area indicates the tapetal region. (B) Quantification of the levels of endogenous canine RHO RNA remaining in the treated retinal area as a percentage of levels measured in the untreated area of eyes injected with different titers. (C) Representative immunoblot and quantification of the levels of endogenous canine RHO protein remaining in the treated retinal area as a percentage of levels measured in the untreated area of eyes injected with 1×10^{11} to 50×10^{11} vg/mL titers. (D) ONL thickness topography 2 wk post light exposure (8–10 wk postinjection) in four RHO-mutant dog eyes treated with 1×10^{11} to 10×10^{11} vg/mL titers. Dotted lines indicate bleb boundaries; dashed lines indicate ONL rescue boundaries. (Insets) Maps of significance showing retinal regions with ONL thickness (Left) and IS/OS intensity (Right) values compared point by point to the 99th percentile CIs of uninjected controls. (E) Microphotographs of H&E-stained (Upper) and rhodopsin (RHO, green)/human cone arrestin (hCA, red) coimmunolabeled (Lower) retinal cryosections showing morphology of the ONL and outer segment (OS) 2 wk post light exposure (8–10 wk postinjection) in areas treated with 1×10^{11} to 10×10^{11} vg/mL titer range (Tx) and untreated areas (UnTx) of the eyes shown in D.

$(2.5 \times 10^{11}$ and 1×10^{11} vg/mL) had limited or no ONL retention in the treated area (Fig. 3D). Histological analysis of these eyes (Fig. 3E) confirmed the results of in vivo retinal imaging. There was ONL retention with shortened inner segments, loss of outer segment structure, and reduction in rod opsin immunolabeling following injection with the two highest titers. (Note: Some variability in the amounts of remaining RHO was observed by immunohistochemistry; panels in Fig. 3E show areas with highest RHO immunolabeling.) In the eye injected with the 10×10^{11} vg/mL titer, cell infiltrates were seen in the inner retina (Fig. 3E, Upper), around retina vessels, and in the subretinal space and choroid of the treated area. With the 2.5×10^{11} vg/mL titer severe ONL thinning was found within the treated area with the exception of a small island of ONL retention. The lowest $(1 \times 10^{11}$ vg/mL) titer did not confer any protection against light exposure. In this eye, the ONL in the treated area resembled that of the untreated region; it was limited to a single row of cone somata with rare residual rod somata and rod opsin-positive debris.

Taken together these findings confirm that $shRNA_{820}$ can suppress both WT and T4R alleles in vivo and that AAV2/5-$shRNA_{820}$ titers in the 5×10^{11} to 10×10^{11} vg/mL range confer protection of photoreceptor cells (but not their outer segments) from retinal degeneration in *RHO*-mutant retinas. This partial protective effect likely results from efficient RHO suppression which leads to deconstruction of rod outer segments while keeping the inner segments and rod photoreceptor cell bodies intact. The need to protect the retina from mutant *RHO*-driven degeneration while retaining functional rods that have preserved light-sensing outer segments led us next to explore whether the suppression of endogenous canine RHO (WT and mutant) could be supplemented with the expression of human RHO cDNA (RHO_{820}) made resistant to $shRHA_{820}$.

Combined Suppression and Replacement.

Dual-vector/dual-function strategy.
We initially tested a two-vector strategy by coinjecting the AAV-$shRNA_{820}$ used above with a similar AAV2/5 serotype carrying the resistant human RHO cDNA (RHO_{820}) under the control of the human opsin promoter (AAV-RHO_{820}). Two *RHO*-mutant eyes were coinjected with a similar titer (5×10^{11} vg/mL) of both vectors (treatment 1:1), and two other mutant eyes were coinjected with AAV-$shRNA_{820}$ at 5×10^{11} vg/mL and AAV-RHO_{820} at 10×10^{11} vg/mL (treatment 1:2) (*SI Appendix*, Table S1 group G). At 7 wk postinjection one eye in each treatment group was exposed to the light-exposure protocol, and all four eyes were imaged 4 wk later by OCT. In the light-exposed eye receiving treatment 1:1, there was some ONL retention, but it did not reach normal thickness in most of the treated area (*SI Appendix*, Fig. S7A). In the region with the greatest ONL retention, there was some rod outer segment preservation suggesting a beneficial outcome conferred by replacement with RHO_{820} (*SI Appendix*, Fig. S7 B and C). Partial ONL protection also occurred in the light-exposed eye that had received treatment 1:2; however, abnormally increased thickness of the inner retina was seen in the treated region (*SI Appendix*, Fig. S7D) resulting from severe perivascular and inner retinal infiltration of mononuclear inflammatory cells (*SI Appendix*, Fig. S7F). In addition, rod outer segment disruption was present (*SI Appendix*, Fig. S7E). Similar findings that included focal retinal detachment and signs of perivascular, and subretinal cellular infiltration (*SI Appendix*, Fig. S7G) were observed by OCT in the contralateral shielded eye (treatment 1:2). The results of this two-vector strategy pointed toward a beneficial effect of the combination of knockdown and replacement function. Nevertheless, there was incomplete rod protection, and treatment resulted in severe retinal complications. To circumvent these limitations, we developed a single AAV vector that combined the knockdown ($shRNA_{820}$) and resistant replacement (RHO_{820}) elements. We hypothesized that this alternative strategy would ensure

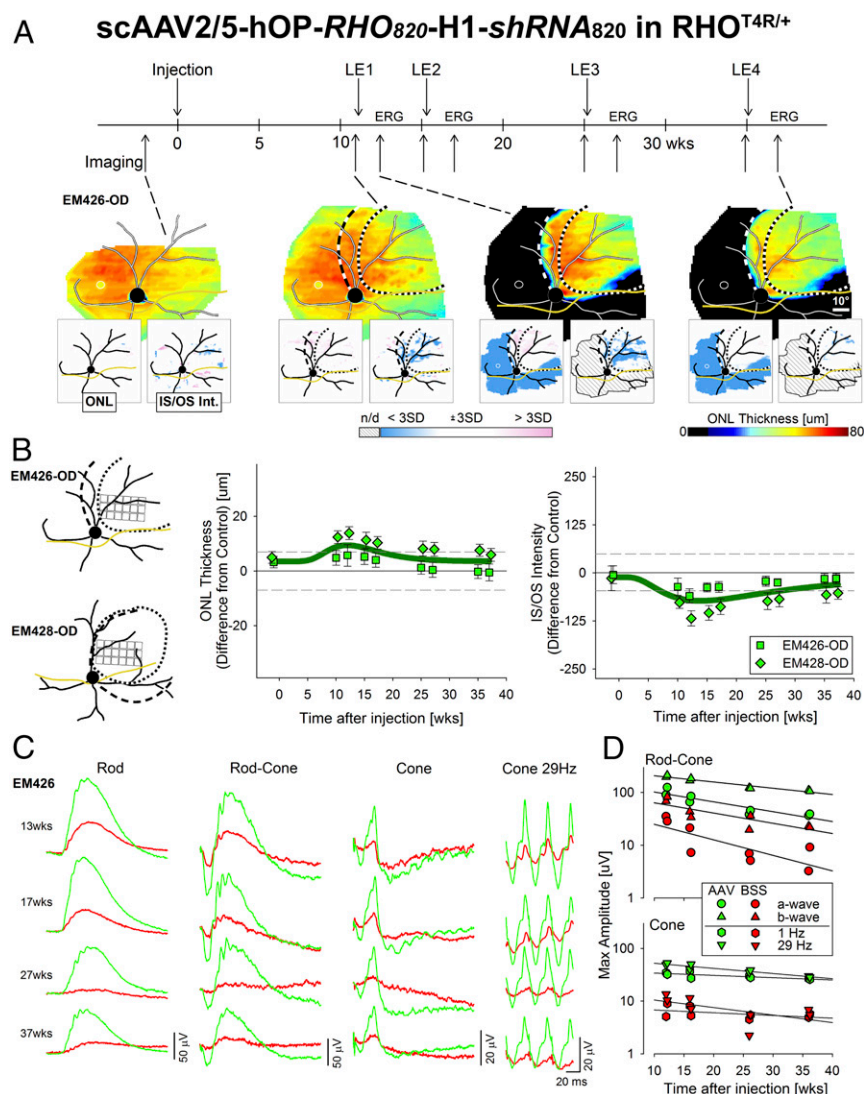## scAAV2/5-hOP-RHO_{820}-H1-$shRNA_{820}$ in RHO$^{T4R/+}$
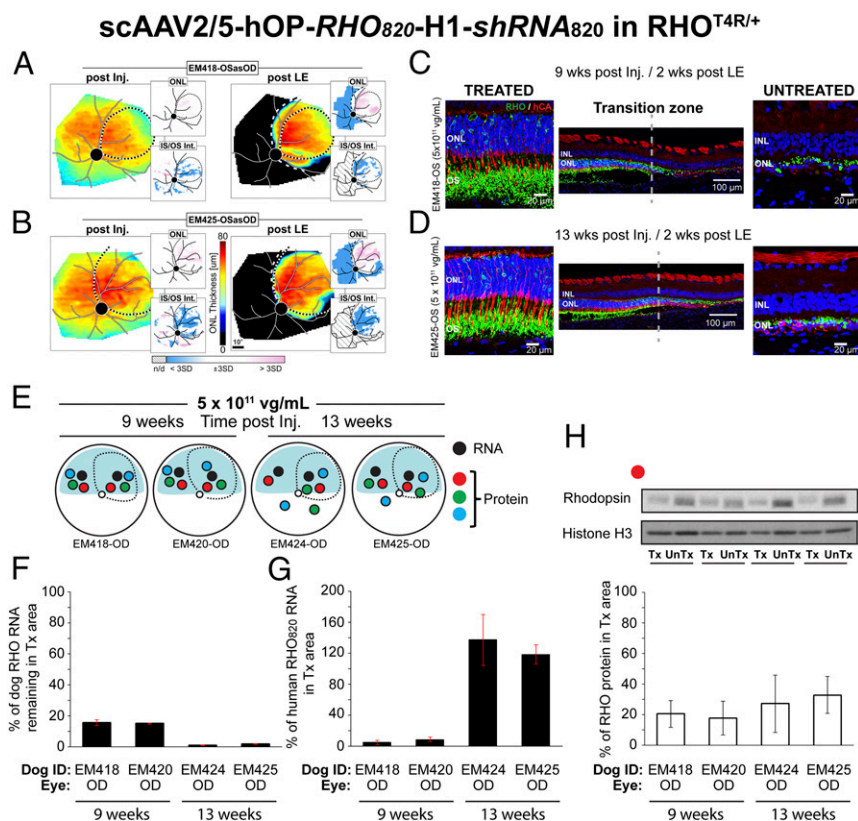
Fig. 4. Suppression and replacement of rhodopsin with a single vector prevents retinal degeneration in *RHO*-mutant retinas. (*A* and *B*) ONL thickness topography after injection/before light exposure (post Inj.) and 2 wk post light exposure (post LE) in two *RHO*-mutant eyes injected with scAAV2/5-hOP-RHO_{820}-H1-$shRNA_{820}$ at 5×10^{11} vg/mL titer. Dotted lines indicate bleb boundaries; dashed lines indicate ONL rescue boundaries. (*Insets*) Maps of significance as described in Fig. 3. (*C* and *D*) Retinal cryosections coimmunolabeled with rhodopsin (RHO, green)/human cone arrestin (hCA, red) showing morphology of the ONL and outer segment (OS) in treated and untreated areas of the eyes shown in *A* and *B*. (*E*) Schematic representation of the fundus of four *RHO*-mutant dog eyes injected with a 5×10^{11} vg/mL titer showing the location of neuroretinal punches used for quantification of rhodopsin (RNA and protein) expression. Dashed lines indicate bleb boundaries; the blue area indicates the tapetal region. (*F*) Quantification of the levels of endogenous canine RHO RNA remaining in the treated retinal area as a percentage of levels measured in the untreated area of injected eyes. (*G*) Quantification of the levels of exogenous human RHO RNA (RHO_{820}) present in the treated retinal area as a percentage of physiological levels of endogenous canine RHO measured in the untreated area of injected eyes. (*H*) Representative immunoblot and quantification of the levels of total (endogenous canine and RHO_{820}) RHO protein remaining in the treated retinal area as a percentage of levels measured in the untreated area of injected eyes.

cotransduction of photoreceptors at a lower viral load and thus achieve better protection from retinal degeneration and improved safety.

Single-vector/dual-function strategy. A single AAV2/5 vector was developed to express both $shRNA_{820}$ under control of the H1 RNA promoter and the human replacement rhodopsin cDNA (RHO_{820}) under control of a 536-bp region of the human rhodopsin proximal promoter. These components were cloned between AAV2 inverted terminal repeats (ITRs), with the terminal resolution site deleted from the ITR close to the shRNA (*SI Appendix*, Fig. S10) (50). Subretinal injections of AAV-$shRNA_{820}$-RHO_{820} were performed in eight *RHO*-mutant eyes at the previously determined optimal titer of 5×10^{11} vg/mL (*SI Appendix*, Table S1 group H). Treated animals were subjected to the light-exposure protocol at 7 wk (*n* = 2 eyes) or at 13 wk (*n* = 2 eyes) postinjection to determine the efficacy of the single-vector approach in preventing acute retinal degeneration. In all four eyes there was substantial retention of ONL thickness 2 wk after light exposure (Fig. 4 *A* and *B* and *SI Appendix*, Fig. S8 *A* and *B*). Most significantly, all four eyes had a detectable IS/OS signal in the treated area. Structural analysis of photoreceptors by immunohistochemistry (Fig. 4 *C* and *D* and *SI Appendix*, Fig. S8 *C* and *D*) confirmed the in vivo results: In treated areas a normal number of photoreceptor cell bodies were retained in the ONL, and rod outer segments were detected. Preservation of

elongated rod outer segments was associated with improved morphology of cone inner and outer segments. Four contralateral eyes that had been injected with a similar dose of AAV-$shRNA_{820}$-RHO_{820} but not exposed to light were collected at similar time points (9 and 13 wk postinjection) and were processed for RHO RNA and protein quantification in treated and untreated areas (Fig. 4*E*). As anticipated, canine RHO RNA (Fig. 4*F*) at 9 wk postinjection was considerably reduced in the treated areas of the two eyes, to 15–16% of that found in untreated areas. In the two eyes that were processed at 13 wk postinjection, the levels of remaining canine *RHO* RNA were further reduced to 1–2% of the levels in untreated areas. The human RHO_{820} transgene transcript levels (Fig. 4*G*) in the two eyes collected at 9 wk postinjection were at 5–9% of canine *RHO* levels measured in untreated areas. At a later time point, 13 wk postinjection, the levels of human RHO_{820} RNA were considerably higher, 118–132% of canine *RHO* levels measured in untreated areas. At the protein level (Fig. 4*H*), measurements of total (endogenous canine and human) RHO protein showed a similar temporal trend, with higher RHO protein levels at 13 wk than at 9 wk postinjection (31–33% vs. 18–19% of the canine RHO levels in untreated areas, respectively). Taken together, these results confirm that a single viral vector that combines both a RHO knockdown and RHO replacement function can effectively preserve the integrity of the entire structure of the rod

Fig. 5. Long-term protection of retinal structure and function in *RHO*-mutant retinas treated with a single vector that combines suppression and replacement of rhodopsin. (*A*, *Upper*) Timeline showing time points of injection of scAAV2/5-hOP-RHO_{820}-H1-$shRNA_{820}$ (5×10^{11} vg/mL titer) in one eye of two *RHO*-mutant dogs (the contralateral eye was injected with BSS), light exposures (LE1–LE4), OCT imaging, and ERG sessions. (*Lower*) Representative ONL thickness maps before injection, 11 wk postinjection (immediately before LE1), 1.5 wk post LE1, and 2.1 wk post LE4 of an eye injected with scAAV2/5-hOP-RHO_{820}-H1-$shRNA_{820}$. Dotted and dashed lines as described in Fig. 4. The optic nerve head (black), major blood vessels (white), tapetum boundary (yellow), and fovea-like region (white ellipse) are overlaid. (*Insets*) Maps of significance as described in Fig. 3. (*B*, *Left*) Schematics showing retinal locations sampled for quantification of ONL thickness and IS/OS intensity within the treated area of two RHO mutant eyes injected with scAAV2/5-hOP-RHO_{820}-H1-$shRNA_{820}$. (*Middle* and *Right*) Longitudinal quantification of the mean (± SD) difference in ONL thickness (*Middle*) and IS/OS intensity (*Right*) in the injected eyes compared with uninjected controls. Horizontal dashed lines represent limits of WT variability (± 3 SD). (*C*) Representative ERG traces of rod [−1.7 log candela (cd)·s·m^{-2}], mixed rod–cone (0.51 log cd·s·m^{-2}) recorded in dark-adapted eyes, and cone responses to single stimuli (0.51 log cd·s·m^{-2}) or to 29-Hz flicker (0.26 log cd·s·m^{-2}) recorded in light-adapted eyes at ~2 wk after each of four light-exposure sessions in a *RHO*-mutant dog injected with scAAV2/5-hOP-RHO_{820}-H1-$shRNA_{820}$ (green) in one eye and with BSS (red) in the contralateral eye. (*D*) Longitudinal quantification of maximal amplitudes of mixed rod–cone a- and b-waves (*Upper*) and of cone responses to 1-Hz and 29-Hz flicker (*Lower*) in two *RHO*-mutant dogs injected in one eye with scAAV2/5-RHO_{820}-$shRNA_{820}$ (green) and in the contralateral eye with BSS (red) at time points similar to those shown in *C*.

photoreceptors, including their inner and outer segments, and that the levels of expression of the resistant RHO transgene continue to rise several weeks after delivery of the vector.

Long-Term Preservation of Retinal Structure and Function with Single-Vector Treatment. To assess the long-term stability of the single-vector strategy and its ability to protect *RHO*-mutant eyes from degeneration, two *RHO*-mutant dogs were subretinally injected in one eye with AAV-shRNA$_{820}$-RHO$_{820}$ at the previously determined optimal titer of 5×10^{11} vg/mL, while the contralateral eyes received a similar volume of balanced salt solution (BSS) (*SI Appendix*, Table S1 group I). All four eyes were repeatedly light exposed at 11, 15, 25, and 35 wk postinjection. OCT imaging was performed preinjection as well as immediately before and ~2 wk after each light exposure (Fig. 5A, *Upper*, timeline). After the first light exposure, there was complete preservation of photoreceptors within the treated area, and this dramatic treatment effect persisted for 37 wk post injection, even after three additional light exposures (Fig. 5A, *Lower*). Quantitative analysis performed in sampled retinal locations (Fig. 5B, *Left*) from the treated area of the two AAV-shRNA$_{820}$-RHO$_{820}$–injected eyes showed a small increase in ONL thickness after injection that peaked near 12 wk before gradually returning to normal levels by 37 wk (Fig. 5B, *Center*). IS/OS signal remained detectable within the treated areas at all time points. There was, a slight decrease in IS/OS intensity that also peaked near 12 wk followed by a gradual return to normal levels by 37 wk postinjection (Fig. 5B, *Right*).

Electroretinography (ERG) measurements were performed 2.1–2.4 wk after each light exposure to assess retinal function (Fig. 5A, *Upper*, timeline). Qualitatively, ERGs of a *RHO*-mutant dog showed consistently better rod- and cone-mediated function in the AAV-shRNA$_{820}$-RHO$_{820}$–treated eye (Fig. 5C, green traces) than in the contralateral BSS-injected eye (Fig. 5C, red traces); substantial ERG asymmetry was present between vector and BSS-treated eyes, and the asymmetry increased after each light exposure (Fig. 5C). Quantitatively, amplitudes of rod-dominated ERG traces showed a tendency to decrease over time in both the AAV- and BSS-injected eyes, likely due to continued photoreceptor degeneration occurring in the peripheral retina outside treatment areas (Fig. 5D, *Upper*). Cone function appeared overall to be more stable throughout the 37-wk postinjection period with four intervening light exposures (Fig. 5D, *Lower*). Importantly, at each time point there were substantially greater rod and cone responses in treated eyes.

These results demonstrate that AAV-shRNA$_{820}$-RHO$_{820}$ preserves the integrity of the entire structure of rod photoreceptors and confers long-term protection of retinal structure and function from the degeneration that otherwise occurs rapidly in untreated *RHO*-mutant eyes.

Discussion

Despite considerable efforts at developing gene therapies for autosomal dominant diseases (51), only two involving antisense technology (antisense oligonucleotide and siRNA) have reached the clinical trial stage (NCT01041222 and NCT02363946), and these are for systemic diseases without a retinal phenotype. The development of mutation-independent gene knockdown-and-replacement approaches have been explored for the treatment of dominantly inherited systemic and retinal diseases that result from toxic gain-of-function mutations and/or to circumvent high mutational heterogeneity (40–43, 52, 53). A significant challenge that likely has delayed the development of clinical therapies is the need to successfully fine-tune the level of reduction of both mutant and WT endogenous proteins while providing sufficient resistant replacement (54). Here, we show in a naturally occurring large animal form of *RHO*-adRP that this dual-function strategy can effectively provide long-term photoreceptor pres-

ervation. In addition, we show that when both knockdown and replacement components are codelivered in the same viral vector, they provide increased efficacy and a better safety profile than when delivered separately.

Rapid Assessment of Gene Therapy Efficacy in a Naturally Occurring Large-Animal Model of *RHO*-adRP. Genetic approaches that include gene augmentation, mutation-dependent *RHO* suppression, and mutation-independent *RHO* knockdown and replacement have been tested to date only in transgenic animal models of *RHO*-adRP. These include the hP23H mouse (5, 41, 43), the hP347S mouse (36, 38, 42, 55), and the mP23H (lines 1 and 3) rat (22, 23, 25, 26, 33). The use of animal models that have different ratios of mutant transgene to endogenous *RHO* copy numbers complicates comparisons of photoreceptor rescue outcomes among these studies and precludes estimating their potential efficiency in the human *RHO*-adRP retina. More recently, a P23H opsin knock-in mouse that expresses equal levels of murine P23H and WT RHO was generated (56). However, this model would have had no use in the current study, as the target site for shRNA$_{820}$ in canine and human *RHO* RNA is not conserved in the mouse.

To increase the predictive value of our studies in the context of a future human clinical trial, we used the *RHO* T4R mutant dog, the only naturally occurring model of *RHO*-adRP (57). Besides its translational value for its human-sized eye, and its phenotypic similarities with class B patients (57), the RHO$^{T4R/+}$ dog expresses equal amounts of mutant and WT RHO proteins (58). Both forms traffic normally to the rod outer segments (58) and sustain normal retinal structure and function until progressive areas of photoreceptor loss are detected in the inferior-temporal (*SI Appendix*, Fig. S9) and central retina (57) within the first 2 y of life. Sensitivity to light, which has been recognized in other models of *RHO*-adRP (for review see supporting information table S1 in ref. 47) and suspected in class B patients (19, 45, 59–61), has been well characterized in the canine *RHO* T4R model (45). Capitalizing on this light sensitivity, we previously developed a light-exposure protocol to experimentally trigger a rapid and synchronized loss of photoreceptors and accelerate the natural disease course (46). *RHO*-mutant (but not WT) dogs undergo a complete loss of rods in the central to midperipheral retina within 2 wk following an acute (1-min) light exposure using intensity levels encountered in clinical patient settings (47, 48). Here, we used this disease-acceleration approach to obtain a rapid read-out of the effect of gene therapy intervention in preventing rod degeneration in *RHO*-mutants. Comparability of the molecular pathophysiology between the natural disease and light-accelerated disease (46, 48, 62) remains to be determined.

RHO Suppression: The Need for a Potent Knockdown Component. Evidence from several animal model studies suggests that a toxic gain-of-function mechanism is associated with a number of *RHO* mutations including P23H (56, 63, 64), T17M (65, 66), and T4R/T4K (45, 66). This toxicity may be exacerbated following exposure to light in many *RHO*-adRP models including the *RHO*-mutant dog (see supporting information table S1 in ref. 47). Thus, we posited that under normal ambient illumination, the T4R mutation produces a protein that is highly toxic once bleached but is stable when bound to chromophore (58) and that efficient protection of rods would require significant knockdown of the mutant transcript. This study examined the efficiency of several *RHO*-knockdown reagents, including three shRNAs and a hammerhead ribozyme, with the goal of identifying the most potent reagent capable of suppressing RHO expression. *Rz525* tested in the *RHO*-mutant dog produced a 64% reduction in endogenous canine RHO protein that was not sufficient to confer protection from light-induced retinal degeneration (*SI Appendix*, Fig. S4 *C* and *D*). This confirmed the high toxicity of

NEUROSCIENCE

the native mutant T4R protein, since remaining amounts as low as 18% of physiological levels of RHO were sufficient to cause disease in a heterozygous mutant retina, and argued for the need to achieve more efficient suppression. When a complete suppression of RHO protein was obtained with *Rz525*, some ONL rescue was observed, but the need for a high viral titer (10^{13} vg/mL) was associated with severe retinal inflammation (*SI Appendix,* Fig. S4 *C–E*). Based on these results, only the most efficient shRNA (*shRNA$_{820}$*) identified in vitro and following screening and testing in WT dogs was subsequently evaluated in mutants. Results confirmed that optimal preservation occurred only when nearly complete suppression of RHO protein expression was achieved, whereas 86% knockdown of RHO provided only partial protection (Fig. 3 *C* and *D*). Some of the most efficient knockdown reagents reported to date have achieved a 90–95% suppression of human *RHO* RNA, but these results were obtained on FACS-sorted transduced rods (36, 41). Here, we intentionally measured the levels of remaining *RHO* RNA and protein from biopsy punches of neuroretina collected within the treated area rather than from an enriched population of transduced rods. Our results show a nearly complete knockdown of RHO message and product in *RHO*-mutant retinas (Fig. 3 *B, C,* and *E*), suggesting not only that *shRNA$_{820}$* is extremely potent but also that rod transduction efficiency was very high. Importantly, this was achieved with an AAV2/5 titer as low as 5×10^{11} vg/mL, which previously has been shown to be within the range of well-tolerated titers in dog retinas (44, 67, 68). The nearly complete suppression of RHO protein expression in WT and *RHO*-mutant dogs was associated with a loss of the outer segment, similar to the collapse of rod outer segment structure reported by others (36, 55). It is important to note that suppression of RHO was not associated with any reduction in ONL thickness, suggesting that rods can survive for at least 10 wk following administration of *shRNA$_{820}$*. This interval provides a window for concomitant expression of a resistant *RHO* replacement component to produce sufficient protein to prevent outer segment deconstruction or initiate outer segment regeneration.

RHO Replacement: How Much Is Enough, and How Much Is Too Much?
As little as 23% overexpression of rhodopsin has been shown to cause retinotoxicity in transgenic mice (69, 70), thus calling for tight regulation of *RHO* gene-supplementation strategies. However, retinal degeneration was not observed when *RHO* gene augmentation was delivered postnatally in the hP23H *RHO$^{+/-}$*, *mRHO$^{+/+}$* transgenic mouse. This genetic configuration led to a twofold increase in RHO RNA and a 58% increase in RHO protein and resulted in both structural and functional rods for up to 6 mo posttreatment (5). These apparently conflicting results suggest that mature rods may tolerate higher levels of RHO overexpression than developing photoreceptors. In the current study, gene augmentation was not considered in the *RHO*-mutant dog because of the highly toxic gain of function of the T4R mutation and also because this strategy had failed to confer protection when tested in the hP23H *RHO$^{+/-}$*, mRHO$^{+/-}$ transgenic mouse that carries one mutant (hP23H) and one WT (mRHO) allele (43). Instead, replacement with a resistant *RHO* cDNA, *RHO$_{820}$*, was evaluated together with *shRNA820*-mediated *RHO* suppression. In the treated areas of mutant retinas injected 9 wk prior with AAV2/5-*shRNA$_{820}$*-*RHO$_{820}$*, total RHO protein levels as low as 18% of that found in untreated regions (Fig. 4*H*) were sufficient to preserve rod outer segment structure (Fig. 4*C* and *SI Appendix,* Fig. S8*C*). When retinas from two additional injected eyes were processed 4 wk later (13 wk postinjection), higher protein amounts (up to 33% of untreated areas) were measured (Fig. 4*H*), which also sustained outer segment formation (Fig. 4*D* and *SI Appendix,* Fig. S8*D*). These findings suggest that the kinetics of RHO replacement are

slower than the kinetics of suppression and that maximal levels of RHO expression may not be reached until several weeks post treatment.

Combining Knockdown and Replacement in a Single Vector Achieves Optimal Efficiency and Improved Safety over a Two-Vector Approach.
Previous efforts at copackaging the knockdown and replacement reagents within a same viral vector provided short-term (10 d postinjection) preservation of ONL thickness but failed to rescue rod outer segment structure in a hP23H *RHO$^{+/-}$*, *mRHO$^{+/-}$* transgenic mouse (41). This led to consideration of a two-vector approach whereby the knockdown and replacement reagents were packaged separately, enabling coadministration of different ratios of the two vectors to better control the levels of *RHO* suppression and replacement. This strategy achieved preservation of ONL thickness, rod outer segment structure, and ERG function in the hP347S *RHO$^{+/-}$*, *mRHO$^{+/-}$* transgenic mouse, but the effect was not sustained (42). In the current study, coinjection of AAV-*shRNA$_{820}$* and AAV-*RHO$_{820}$* led to some degree of protection against light exposure, but signs of severe retinal inflammation were observed, likely because of the combined higher viral doses administered (*SI Appendix,* Fig. S7). This finding led us to pursue the single-vector dual-function strategy that our group previously evaluated successfully in a mouse model (43). *ShRNA$_{820}$* and *RHO$_{820}$* driven respectively by the human H1 RNA and the human opsin proximal promoters were successfully packaged within the cargo capacity limit of the recombinant AAV cassette. The efficiency of this construct remained very high, achieving suppression of ~98.5% of endogenous canine *RHO* RNA at 13 wk post injection and expression of human canine *RHO* at levels comparable to normal. However, at the protein level, replacement resulted in only about a third of normal levels. This discrepancy between RNA and protein levels could be explained by several factors, including the possibility that synonymous codon modifications introduced at wobble/degenerate sites to generate the resistant *RHO$_{820}$* cDNA influenced its translation efficiency. Analysis of codon frequency of the four modified codons at the *RHO* target site of *shRNA$_{820}$* showed for both canine and human *RHO* an increase in frequency for one codon, a decrease in frequency for the three others, and an overall decrease when all four were combined (*SI Appendix,* Table S2). Since a correlation has been found between codon usage and relative tRNA abundance, particularly for highly expressed genes that are tissue specific (71), the introduction of three codons with lower frequency could have led to a reduced rate of RHO$_{820}$ translation (72). Therefore it may be possible to improve rhodopsin expression by reducing the number of modifications in the replacement gene. A single mismatch between an siRNA and an mRNA may be sufficient to block RNA silencing if the mismatch occurs near the RNA-induced silencing complex (RISC)-mediated cleavage site (73). Another possible explanation unrelated to codon bias may be that the kinetics of *RHO* suppression are faster than the kinetics of *RHO* replacement. The H1 RNA polymerase III promoter used in our vector is considered safer than the more potent U6 promoter, which leads to a very high level of shRNA expression and, potentially, to saturation of the processing system for endogenous miRNAs. Nevertheless, H1 RNA is expressed abundantly, and the promoter used here functions in all cell types tested (74, 75). This could explain why at 9 wk postinjection there was already a prominent reduction (~84%) of endogenous *RHO* RNA levels while *RHO$_{820}$* RNA levels reached only 5–9% of normal (Fig. 4 *F* and *G*). While immunohistochemical analysis revealed the presence of RHO protein in the structurally preserved outer segment, retinal OCT imaging of the IS/OS intensity, a surrogate marker of IS/OS integrity, showed that the signal, although detectable, was decreased at 9 and 13 wk postinjection (Fig. 4 *A* and *B* and *SI Appendix,* Fig. S8 *A* and *B*). Longitudinal analysis in

two *RHO*-mutant dogs treated with AAV-*shRNA$_{820}$-RHO$_{820}$* and submitted to four acute light-exposure events showed a similar decline in IS/OS intensity that peaked at ∼12 wk post-injection followed by a gradual and nearly complete recovery by 37 wk.

Functional Assessment. Successful and complete protection of rods was achieved over the long term (37 wk/8.5 mo) following a single subretinal injection of AAV-*shRNA$_{820}$-RHO$_{820}$* in mutants that repeatedly had acute light exposures that cause complete loss of rods in the central to midperipheral retina after just a single event. Substantially improved ERG responses were consistently seen in AAV-treated eyes at all time points. While the cone-mediated ERG response was stable, a slight decline in rod-dominated ERG function was noted. A slight increase in ONL thickness without any clinical evidence of inflammation, as seen in dogs injected with AAV-mediated gene therapy in other studies (76, 77), was also observed here in the treated areas. This increase likely reflects intra- or intercellular swelling due to a transient and subclinical response to the viral vector, since this effect was not seen in the BSS-injected eyes before light exposure or in the natural history of uninjected eyes housed under standard or dim red cyclic illumination (*SI Appendix*, Fig. S9). The return of ONL thickness to normal preinjection values ruled out the hypothesis that the observed ERG decline was associated with photoreceptor loss within the treated regions. Instead, the functional decline is likely explained by the additional loss of rods located in the untreated peripheral retina following cumulative light exposure, and this hypothesis is consistent with the similar decline in rod-dominated ERG amplitudes found in the contralateral BSS-injected eyes.

In summary, we have developed a single vector with dual *RHO* knockdown and replacement functions that provides complete and long-term protection of rods against a class B *RHO* mutation with a toxic gain of function identified in a naturally occurring large-animal model of *RHO*-adRP. This highly efficient mutation-independent strategy raises hope that a common gene therapy for all *RHO*-adRP patients with class B mutations will be an achievable goal.

Material and Methods

In vitro assays conducted in HEK293T (ATCC) cells (33) were used to screen the efficiency of a hammerhead ribozyme (*Rz525*) and three shRNAs (*shRNA$_{131}$*, *shRNA$_{134}$*, and *shRNA$_{820}$*) in suppressing WT and mutant (P23H, T17M) human RHO expression (78). Self-complementary (79) and non–self-complementary AAV vectors were packaged in serotype 5 (80) by double-plasmid DNA transfection and were purified according to previously published methods (81, 82). The titer of DNase-resistant vector genomes was measured by real-time PCR relative to a standard; purity was validated by silver-stained SDS/PAGE, sterility and the absence of endotoxin were confirmed, and aliquots were stored at −80 °C before use. WT and *RHO*-mutant dogs (45, 57) were used to evaluate the response to subretinal injections of AAV2/5 vectors carrying the most potent knockdown reagents, either alone (*Rz525*, *shRNA820*) or in combination (*shRNA820*) with a codon-modified resistant human RHO cDNA (*RH0$_{820}$*) (*SI Appendix*, Fig. S10). Assessment of the effect of *RHO* suppression and replacement was made by means of *en face* and cross-sectional in vivo retinal imaging, ERG, quantification of RHO protein and RNA levels, and morphological evaluation on retinal histological sections (76, 83–85). A light-exposure paradigm (46–48) was used to accelerate the natural course of disease in the *RHO*-mutant dogs and rapidly assess whether the subretinally delivered AAV constructs prevented the onset of retinal degeneration. All dogs were bred and maintained at the University of Pennsylvania Retinal Disease Studies Facility (RDSF). The studies were carried out in strict accordance with the recommendations in the NIH *Guide for the Care and Use of Laboratory Animals* (86) and the US Department of Agriculture Animal Welfare Act and Animal Welfare Regulations and complied with the Association for Research in Vision and Ophthalmology Statement for the Use of Animals in Ophthalmic and Vision Research. The protocols were approved by the Institutional Animal Care and Use Committee of the University of Pennsylvania. Methodological details are provided in *SI Appendix, Supplemental Methods*.

1. Ginn SL, Alexander IE, Edelstein ML, Abedi MR, Wixon J (2013) Gene therapy clinical trials worldwide to 2012–An update. *J Gene Med* 15:65–77.
2. Dunbar CE, et al. (2018) Gene therapy comes of age. *Science* 359:eaan4672.
3. Ferrua F, Aiuti A (2017) Twenty-five years of gene therapy for ADA-SCID: From bubble babies to an approved drug. *Hum Gene Ther* 28:972–981.
4. Kumar SR, Markusic DM, Biswas M, High KA, Herzog RW (2016) Clinical development of gene therapy: Results and lessons from recent successes. *Mol Ther Methods Clin Dev* 3:16034.
5. Mao H, et al. (2011) AAV delivery of wild-type rhodopsin preserves retinal function in a mouse model of autosomal dominant retinitis pigmentosa. *Hum Gene Ther* 22:567–575.
6. Stanton CM, et al. (2017) Novel pathogenic mutations in C1QTNF5 support a dominant negative disease mechanism in late-onset retinal degeneration. *Sci Rep* 7:12147.
7. Lewin AS, Glazer PM, Milstone LM (2005) Gene therapy for autosomal dominant disorders of keratin. *J Investig Dermatol Symp Proc* 10:47–61.
8. Miller TM, et al. (2013) An antisense oligonucleotide against SOD1 delivered intrathecally for patients with SOD1 familial amyotrophic lateral sclerosis: A phase 1, randomised, first-in-man study. *Lancet Neurol* 12:435–442.
9. Bennett J (2017) Taking stock of retinal gene therapy: Looking back and moving forward. *Mol Ther* 25:1076–1094.
10. Hartong DT, Berson EL, Dryja TP (2006) Retinitis pigmentosa. *Lancet* 368:1795–1809.
11. Sung CH, et al. (1991) Rhodopsin mutations in autosomal dominant retinitis pigmentosa. *Proc Natl Acad Sci USA* 88:6481–6485.
12. Inglehearn CF, et al. (1992) A completed screen for mutations of the rhodopsin gene in a panel of patients with autosomal dominant retinitis pigmentosa. *Hum Mol Genet* 1:41–45.
13. Sullivan LS, et al. (2006) Prevalence of disease-causing mutations in families with autosomal dominant retinitis pigmentosa: A screen of known genes in 200 families. *Invest Ophthalmol Vis Sci* 47:3052–3064.
14. Sullivan LS, et al. (2013) Prevalence of mutations in eyeGENE probands with a diagnosis of autosomal dominant retinitis pigmentosa. *Invest Ophthalmol Vis Sci* 54:6255–6261.
15. Athanasiou D, et al. (2018) The molecular and cellular basis of rhodopsin retinitis pigmentosa reveals potential strategies for therapy. *Prog Retin Eye Res* 62:1–23.
16. Sung CH, Davenport CM, Nathans J (1993) Rhodopsin mutations responsible for autosomal dominant retinitis pigmentosa. Clustering of functional classes along the polypeptide chain. *J Biol Chem* 268:26645–26649.
17. Jacobson SG, Kemp CM, Sung CH, Nathans J (1991) Retinal function and rhodopsin levels in autosomal dominant retinitis pigmentosa with rhodopsin mutations. *Am J Ophthalmol* 112:256–271.
18. Jacobson SG, et al. (1994) Phenotypes of stop codon and splice site rhodopsin mutations causing retinitis pigmentosa. *Invest Ophthalmol Vis Sci* 35:2521–2534.
19. Cideciyan AV, et al. (1998) Disease sequence from mutant rhodopsin allele to rod and cone photoreceptor degeneration in man. *Proc Natl Acad Sci USA* 95:7103–7108.
20. Jacobson SG, et al. (2016) Complexity of the class B phenotype in autosomal dominant retinitis pigmentosa due to rhodopsin mutations. *Invest Ophthalmol Vis Sci* 57:4847–4858.
21. Drenser KA, Timmers AM, Hauswirth WW, Lewin AS (1998) Ribozyme-targeted destruction of RNA associated with autosomal-dominant retinitis pigmentosa. *Invest Ophthalmol Vis Sci* 39:681–689.
22. Lewin AS, et al. (1998) Ribozyme rescue of photoreceptor cells in a transgenic rat model of autosomal dominant retinitis pigmentosa. *Nat Med* 4:967–971.
23. LaVail MM, et al. (2000) Ribozyme rescue of photoreceptor cells in P23H transgenic rats: Long-term survival and late-stage therapy. *Proc Natl Acad Sci USA* 97:11488–11493.
24. Shaw LC, et al. (2001) An allele-specific hammerhead ribozyme gene therapy for a porcine model of autosomal dominant retinitis pigmentosa. *Mol Vis* 7:6–13.
25. Tessitore A, et al. (2006) Preferential silencing of a common dominant rhodopsin mutation does not inhibit retinal degeneration in a transgenic model. *Mol Ther* 14:692–699.
26. Murray SF, et al. (2015) Allele-specific inhibition of rhodopsin with an antisense oligonucleotide slows photoreceptor cell degeneration. *Invest Ophthalmol Vis Sci* 56:6362–6375.
27. Bakondi B, et al. (2016) In vivo CRISPR/Cas9 gene editing corrects retinal dystrophy in the S334ter-3 rat model of autosomal dominant retinitis pigmentosa. *Mol Ther* 24:556–563.
28. Burnight ER, et al. (2017) Using CRISPR-Cas9 to generate gene-corrected autologous iPSCs for the treatment of inherited retinal degeneration. *Mol Ther* 25:1999–2013.

NEUROSCIENCE

29. Millington-Ward S, et al. (1997) Strategems in vitro for gene therapies directed to dominant mutations. *Hum Mol Genet* 6:1415–1426.
30. O'Neill B, et al. (2000) Ribozyme-based therapeutic approaches for autosomal dominant retinitis pigmentosa. *Invest Ophthalmol Vis Sci* 41:2863–2869.
31. Sullivan JM, Pietras KM, Shin BJ, Misasi JN (2002) Hammerhead ribozymes designed to cleave all human rod opsin mRNAs which cause autosomal dominant retinitis pigmentosa. *Mol Vis* 8:102–113.
32. Gorbatyuk MS, Pang JJ, Thomas J, Jr, Hauswirth WW, Lewin AS (2005) Knockdown of wild-type mouse rhodopsin using an AAV vectored ribozyme as part of an RNA replacement approach. *Mol Vis* 11:648–656.
33. Gorbatyuk M, Justilien V, Liu J, Hauswirth WW, Lewin AS (2007) Preservation of photoreceptor morphology and function in P23H rats using an allele independent ribozyme. *Exp Eye Res* 84:44–52.
34. Gorbatyuk M, Justilien V, Liu J, Hauswirth WW, Lewin AS (2007) Suppression of mouse rhodopsin expression in vivo by AAV mediated siRNA delivery. *Vision Res* 47:1202–1208.
35. O'Reilly M, et al. (2008) A transgenic mouse model for gene therapy of rhodopsin-linked retinitis pigmentosa. *Vision Res* 48:386–391.
36. Chadderton N, et al. (2009) Improved retinal function in a mouse model of dominant retinitis pigmentosa following AAV-delivered gene therapy. *Mol Ther* 17:593–599.
37. Abdelmaksoud HE, Yau EH, Zuker M, Sullivan JM (2009) Development of lead hammerhead ribozyme candidates against human rod opsin mRNA for retinal degeneration therapy. *Exp Eye Res* 88:859–879.
38. Mussolino C, et al. (2011) Zinc-finger-based transcriptional repression of rhodopsin in a model of dominant retinitis pigmentosa. *EMBO Mol Med* 3:118–128.
39. Latella MC, et al. (2016) In vivo editing of the human mutant rhodopsin gene by electroporation of plasmid-based CRISPR/Cas9 in the mouse retina. *Mol Ther Nucleic Acids* 5:e389.
40. Kiang AS, et al. (2005) Toward a gene therapy for dominant disease: Validation of an RNA interference-based mutation-independent approach. *Mol Ther* 12:555–561.
41. O'Reilly M, et al. (2007) RNA interference-mediated suppression and replacement of human rhodopsin in vivo. *Am J Hum Genet* 81:127–135.
42. Millington-Ward S, et al. (2011) Suppression and replacement gene therapy for autosomal dominant disease in a murine model of dominant retinitis pigmentosa. *Mol Ther* 19:642–649.
43. Mao H, Gorbatyuk MS, Rossmiller B, Hauswirth WW, Lewin AS (2012) Long-term rescue of retinal structure and function by rhodopsin RNA replacement with a single adeno-associated viral vector in P23H RHO transgenic mice. *Hum Gene Ther* 23:356–366.
44. Beltran WA, et al. (2017) Optimization of retinal gene therapy for X-linked retinitis pigmentosa due to RPGR mutations. *Mol Ther* 25:1866–1880.
45. Cideciyan AV, et al. (2005) In vivo dynamics of retinal injury and repair in the rhodopsin mutant dog model of human retinitis pigmentosa. *Proc Natl Acad Sci USA* 102:5233–5238.
46. Marsili S, et al. (2015) Exclusion of the unfolded protein response in light-induced retinal degeneration in the canine T4R RHO model of autosomal dominant retinitis pigmentosa. *PLoS One* 10:e0115723.
47. Iwabe S, Ying GS, Aguirre GD, Beltran WA (2016) Assessment of visual function and retinal structure following acute light exposure in the light sensitive T4R rhodopsin mutant dog. *Exp Eye Res* 146:341–353.
48. Sudharsan R, Simone KM, Anderson NP, Aguirre GD, Beltran WA (2017) Acute and protracted cell death in light-induced retinal degeneration in the canine model of rhodopsin autosomal dominant retinitis pigmentosa. *Invest Ophthalmol Vis Sci* 58:270–281.
49. Komáromy AM, Acland GM, Aguirre GD (2008) Operating in the dark: A night-vision system for surgery in retinas susceptible to light damage. *Arch Ophthalmol* 126:714–717.
50. McCarty DM, et al. (2003) Adeno-associated virus terminal repeat (TR) mutant generates self-complementary vectors to overcome the rate-limiting step to transduction in vivo. *Gene Ther* 10:2112–2118.
51. Pelletier R, Caron SO, Puymirat J (2006) RNA based gene therapy for dominantly inherited diseases. *Curr Gene Ther* 6:131–146.
52. Palfi A, et al. (2006) RNAi-based suppression and replacement of rds-peripherin in retinal organotypic culture. *Hum Mutat* 27:260–268.
53. Mueller C, et al. (2012) Sustained miRNA-mediated knockdown of mutant AAT with simultaneous augmentation of wild-type AAT has minimal effect on global liver miRNA profiles. *Mol Ther* 20:590–600.
54. Conley SM, Naash MI (2014) Gene therapy for PRPH2-associated ocular disease: Challenges and prospects. *Cold Spring Harb Perspect Med* 4:a017376.
55. Botta S, et al. (2016) Rhodopsin targeted transcriptional silencing by DNA-binding. *eLife* 5:e12242.
56. Sakami S, et al. (2011) Probing mechanisms of photoreceptor degeneration in a new mouse model of the common form of autosomal dominant retinitis pigmentosa due to P23H opsin mutations. *J Biol Chem* 286:10551–10567.
57. Kijas JW, et al. (2002) Naturally occurring rhodopsin mutation in the dog causes retinal dysfunction and degeneration mimicking human dominant retinitis pigmentosa. *Proc Natl Acad Sci USA* 99:6328–6333.

58. Zhu L, et al. (2004) A naturally occurring mutation of the opsin gene (T4R) in dogs affects glycosylation and stability of the G protein-coupled receptor. *J Biol Chem* 279:53828–53839.
59. Heckenlively JR, Rodriguez JA, Daiger SP (1991) Autosomal dominant sectoral retinitis pigmentosa. Two families with transversion mutation in codon 23 of rhodopsin. *Arch Ophthalmol* 109:84–91.
60. Iannaccone A, et al. (2006) Retinitis pigmentosa associated with rhodopsin mutations: Correlation between phenotypic variability and molecular effects. *Vision Res* 46:4556–4567.
61. Paskowitz DM, LaVail MM, Duncan JL (2006) Light and inherited retinal degeneration. *Br J Ophthalmol* 90:1060–1066.
62. Gu D, Beltran WA, Li Z, Acland GM, Aguirre GD (2007) Clinical light exposure, photoreceptor degeneration, and AP-1 activation: A cell death or cell survival signal in the rhodopsin mutant retina? *Invest Ophthalmol Vis Sci* 48:4907–4918.
63. Sakami S, Kolesnikov AV, Kefalov VJ, Palczewski K (2014) P23H opsin knock-in mice reveal a novel step in retinal rod disc morphogenesis. *Hum Mol Genet* 23:1723–1741.
64. Haeri M, Knox BE (2012) Rhodopsin mutant P23H destabilizes rod photoreceptor disk membranes. *PLoS One* 7:e30101.
65. White DA, Fritz JJ, Hauswirth WW, Kaushal S, Lewin AS (2007) Increased sensitivity to light-induced damage in a mouse model of autosomal dominant retinal disease. *Invest Ophthalmol Vis Sci* 48:1942–1951, and erratum (2007) 48:3436.
66. Tam BM, Moritz OL (2009) The role of rhodopsin glycosylation in protein folding, trafficking, and light-sensitive retinal degeneration. *J Neurosci* 29:15145–15154.
67. Beltran WA, et al. (2010) rAAV2/5 gene-targeting to rods: Dose-dependent efficiency and complications associated with different promoters. *Gene Ther* 17:1162–1174.
68. Komáromy AM, et al. (2013) Transient photoreceptor deconstruction by CNTF enhances rAAV-mediated cone functional rescue in late stage CNGB3-achromatopsia. *Mol Ther* 21:1131–1141.
69. Olsson JE, et al. (1992) Transgenic mice with a rhodopsin mutation (Pro23His): A mouse model of autosomal dominant retinitis pigmentosa. *Neuron* 9:815–830.
70. Tan E, et al. (2001) The relationship between opsin overexpression and photoreceptor degeneration. *Invest Ophthalmol Vis Sci* 42:589–600.
71. Dittmar KA, Goodenbour JM, Pan T (2006) Tissue-specific differences in human transfer RNA expression. *PLoS Genet* 2:e221.
72. Gardin J, et al. (2014) Measurement of average decoding rates of the 61 sense codons in vivo. *eLife* 3:e03735.
73. Trochet D, Prudhon B, Vassilopoulos S, Bitoun M (2015) Therapy for dominant inherited diseases by allele-specific RNA interference: Successes and pitfalls. *Curr Gene Ther* 15:503–510.
74. Myslinski E, Amé JC, Krol A, Carbon P (2001) An unusually compact external promoter for RNA polymerase III transcription of the human H1RNA gene. *Nucleic Acids Res* 29:2502–2509.
75. Wu MT, et al. (2005) Simple and efficient DNA vector-based RNAi systems in mammalian cells. *Biochem Biophys Res Commun* 330:53–59.
76. Beltran WA, et al. (2015) Successful arrest of photoreceptor and vision loss expands the therapeutic window of retinal gene therapy to later stages of disease. *Proc Natl Acad Sci USA* 112:E5844–E5853.
77. Guziewicz KE, et al. (2018) BEST1 gene therapy corrects a diffuse retina-wide microdetachment modulated by light exposure. *Proc Natl Acad Sci USA* 115:E2839–E2848.
78. Kunte MM, et al. (2012) ER stress is involved in T17M rhodopsin-induced retinal degeneration. *Invest Ophthalmol Vis Sci* 53:3792–3800.
79. McCarty DM, Monahan PE, Samulski RJ (2001) Self-complementary recombinant adeno-associated virus (scAAV) vectors promote efficient transduction independently of DNA synthesis. *Gene Ther* 8:1248–1254.
80. Auricchio A, et al. (2001) Exchange of surface proteins impacts on viral vector cellular specificity and transduction characteristics: The retina as a model. *Hum Mol Genet* 10:3075–3081.
81. Zolotukhin S, et al. (2002) Production and purification of serotype 1, 2, and 5 recombinant adeno-associated viral vectors. *Methods* 28:158–167.
82. Zolotukhin S, Potter M, Hauswirth WW, Guy J, Muzyczka N (1996) A "humanized" green fluorescent protein cDNA adapted for high-level expression in mammalian cells. *J Virol* 70:4646–4654.
83. Beltran WA, et al. (2012) Gene therapy rescues photoreceptor blindness in dogs and paves the way for treating human X-linked retinitis pigmentosa. *Proc Natl Acad Sci USA* 109:2132–2137.
84. Kuznetsova T, Zangerl B, Goldstein O, Acland GM, Aguirre GD (2011) Structural organization and expression pattern of the canine RPGRIP1 isoforms in retinal tissue. *Invest Ophthalmol Vis Sci* 52:2989–2998.
85. Beltran WA, et al. (2014) Canine retina has a primate fovea-like bouquet of cone photoreceptors which is affected by inherited macular degenerations. *PLoS One* 9:e90390.
86. National Research Council (2011) *Guide for the Care and Use of Laboratory Animals* (National Academies, Washington, DC), 8th Ed.